# DESIGN OF A 100 kHz ARRAY USING ELEMENTS WHICH ARE TRANSVERSELY DRIVEN AND IN WHICH 2-DIMENSIONAL SHADING IS USED

P. Atkins, R.L. Mansfield & B.V. Smith
School of Electronic and Electrical Engineering
University of Birmingham

## 1. INTRODUCTION

This paper describes a multi-element acoustic array designed to operate at a frequency of 100kHz with a controlled sidelobe level performance. The array was specified to have a beamwidth of 5 degrees by 20 degrees with a sidelobe level approaching -30dB. This specification resulted in the construction of an array containing in excess of 100-elements shaded by a Dolph-Chebyshev window function. Each element consisted of a bar driven in a transverse manner. An iterative optimization procedure was used to discard elements and to minimize the number of weights used in the final design.

## 2. THEORETICAL CONSIDERATIONS OF TRANSVERSELY DRIVEN ELEMENTS

In a transversely driven piezoceramic bar, the bar is poled and electrically driven across its width, but its resonant frequency is determined by its length. The advantage of this is that a piezoceramic element, nominally resonant at 100kHz, can be simply and relatively cheaply obtained, without the need for a sandwich structure. The coupling factor for the transverse drive is less than for the conventional drive, but this is not a limitation in narrow band applications.

The equivalent circuit of a transversely driven bar is given elsewhere [1]. In the derivation of this equivalent circuit the assumptions made are, that the lateral dimensions of the bar are small as compared with its length and that the lateral boundaries are stress free. The resonant frequency of the fundamental length mode of an air-backed bar of length l becomes:-

$$f_0 = \frac{c_b}{2l}$$

where $c_b$ is the bar velocity in the piezoceramic, which is given by:-

$$c_b = \sqrt{\frac{1}{\rho_b s^E_{11}}}$$

## 100 kHz ARRAY USING TRANSVERSELY DRIVEN ELEMENTS AND 2-DIMENSIONAL SHADING

For PZT-4 [2]:-

$$\rho_b = 7.5 \times 10^3 \quad kg \quad m^{-3}$$

$$\& \quad s_{11}^E = 12.3 \times 10^{-12} \quad m^2 \quad N^{-1}$$

Therefore the velocity in the PZT-4 bar becomes:-

$$c_b = 3.29 \times 10^3 \quad m \quad s^{-1}$$

and the resonant frequency per mm length is:-

$$f_0 = 1.65 \quad MHz \quad mm^{-1}$$

So a bar of length 16.5 mm would give 100kHz. In practice a standard bar of 15mm was readily available, which gives a predicted unloaded resonance of 109.8kHz. This met the frequency specification for the particular application and so the standard bar was selected.

The 15mm length bar chosen had a square cross-section with a side dimension of 5mm. The radiation impedance, $Z_R$, for an isolated element of square cross-section in a baffle is given by [3]:-

$$Z_R = \rho_w c_w A[R_1(k\sqrt{A}) + jX_1(k\sqrt{A})]$$

where $R_1(k\sqrt{A})$ & $X_1(k\sqrt{A})$ are piston impedance functions, k is the wavenumber, A is the face area and $\rho_w c_w$ is the specific acoustic impedance of water. For a face area of $25 \ mm^2$ and for a frequency of 110 kHz, then $k\sqrt{A} = 2.3$ and the piston impedance functions become:-

$$R_1 = 0.628$$

$$X_1 = 0.675$$

Therefore the radiation impedance becomes:-

$$Z_r = 23.6 + j25.3 \quad mech.\Omega.$$

## 100 kHz ARRAY USING TRANSVERSELY DRIVEN ELEMENTS AND 2-DIMENSIONAL SHADING

When mounted in an array the impedance would be expected to be somewhat different to this. However, for the array layout used the packing factor, defined as the ratio of the area of the element to the area of the array occupied by the element, is low, typically 0.25 and therefore the above value of the impedance will be assumed approximately applicable.

The loaded Q-factor, $Q_L$ , may be shown to be expressible as:-

$$Q_L = \frac{Q_2 + X_1}{\left(\frac{Q_2}{Q_0} + R_1\right)}$$

where $Q_2 = \frac{\pi}{2}\frac{\rho_b c_b}{\rho_w c_w}$ and $Q_0$ is the unloaded Q-factor.

Figure 1a shows the circle diagrams for a PZT-4, 15mm bar in air and water and figure 1b shows the corresponding conductance values. The measurement in water was taken with the front face of the bar just slightly immersed and left overnight to ensure it was properly wetted. From these measurements the unloaded Q-factor, $Q_0$ , is 291 and the resonant frequency in air, $f_0$ , is 107.2kHz. This latter value is within 3% of the value predicted previously. The radiation mass may be calculated from the impedance; using this, the mass of the bar and the measured unloaded resonant frequency, the resonant frequency in water is predicted to be 105.8kHz. This is in good agreement with the measured value of 105.6kHz.

For PZT-4 the value of $Q_2$ becomes 25.8. Using this and the measured unloaded Q-factor the loaded Q-factor, employing the expression quoted above, is predicted to be 37.2, which compares favourably with the measured value of 39.9 taken from figure 1b. From these air and water measurements the unmounted efficiency of the element was estimated to be 85%.

The elements were mounted in suitably machined expanded PVC and a thin layer of epoxy resin was used to cover the front face. Details of the array construction will be outlined during the presentation, but figure 2 shows a cross-sectional view of the mounted array. The lateral loading of the bar by the PVC was not expected to modify unduly the performance of the element.

# 100 kHz ARRAY USING TRANSVERSELY DRIVEN ELEMENTS AND 2-DIMENSIONAL SHADING

## 3. TWO-DIMENSIONAL SHADING FUNCTIONS

The transducer housing and element mounting was machined on a numerically controlled milling machine. This, combined with the low-cost of the transversely driven elements enabled a large number of elements to be used in the design. Conversely, a large number of element weights is both costly and technically difficult to produce. The design procedure was therefore to select a Dolph-Chebychev weighting function and a large number of elements to produce an overly optimistic performance, to discard and combine groups of elements until the performance was reduced to a pre-defined level. The ultimate sidelobe level performance was to be dictated by the random amplitude and phase variations of the elements.

The design procedure started with a two-dimensional Dolph-Chebyshev weighting function with a sidelobe level of -40dB. To avoid the appearance of diffraction secondaries in the 20 degree axis an inter-element spacing of 0.66$\lambda$ was used. The resulting design required an array of 6 x 22 elements. The symmetrical weighting function would require a total of thirty-three separate amplitude weights.

The second stage was to iteratively discard elements at the corner of the array with a small contribution and to group elements together on a least-mean-squares basis until a degraded sidelobe performance level of -35dB was achieved. The original weights of the elements $W_i$ $(1 < i < 33)$ were grouped into a new set of weights $G_j$ $(1 < j \ll 33)$. Where:

$$G_j = \frac{1}{b-a} \prod_{i=a}^{i=b} W_i$$

where $a, b$ are the first and last indices representing the members of the group. Thus, the mean-squared error for a single group introduced by this operation is

$$mean\text{-}squared \;\; error(j) = \sum_{i=a}^{i=b} (W_i - G_j)^2$$

The members of each group can then be chosen to ensure that the mean-squared errors of each group are approximately equal and that the sum of the errors for all the groups is minimized. Such an iterative procedure is complicated by the discrete nature of each of the element weights, $W_i$. A multi-dimensional search procedure over the possible element groupings is required to minimize the total error for the array weighting function.

## 100 kHz ARRAY USING TRANSVERSELY DRIVEN ELEMENTS AND 2-DIMENSIONAL SHADING

The resulting output from the iterative combination and discarding operation is shown in figure 3. The beam pattern would be expected to be that of an array weighted by the discarded values and the error in the weights convolved with the original ideal array. The discrete nature and symmetry of this error beam-pattern would be expected to result in a number of identifiable sidelobes rather than that of a general sidelobe background. The equivalent error beam pattern for the horizontal axis is shown in figure 4. A total of twenty elements were discarded at the corners of the array, leaving an array populated by elements as shown in figure 5. The elements were assembled into a total of fourteen groups which was considered to be the maximum practical limit for the multi-tap transformer used to derive the amplitude weighting function. The amplitude weight-to-error ratio of this configuration was 33dB.

The ultimate performance of such an array would be expected to be determined by the amplitude and phase errors of the individual elements. Reference [3] provides a description for the performance of an array subject to such errors:

$$\langle D^2(\theta)\rangle = D_0^2(\theta) + \frac{[\delta^2+\Delta^2]}{3.G} \qquad \text{where: } G = \frac{(\sum W_i)^2}{\sum W_i^2}$$

$D_0(\theta)$ is the error free beam pattern, $\langle D(\theta)\rangle$ is the actual beam pattern and $\Delta, \delta$ are the fractional amplitude and phase errors which are assumed to be uniformly distributed.

The characteristics of each of the elements were measured and were found to be approximately normally distributed. The fractional amplitude errors, based on conductance measurements, were of the order of 0.008 and the prediction for the fraction phase errors was 0.12. Converting these values to a form suitable to predict the sidelobe level and using a value for $G$ of 66 results in an expected sidelobe level of -35dB. Thus the errors introduced by the random amplitude and phase errors of the elements should be of the same order as the errors introduced by discarding and grouping the elements.

### 4. RESULTS

Figures 6a and 6b show the beam patterns of the completed array measured at 100kHz. The horizontal -3dB beamwidth was 18.8 degrees and the vertical beamwidth was 5.0 degrees. These values compare well with the design values of 20 degrees by 5 degrees. The horizontal sidelobe level was approximately -26dB and the vertical sidelobe level was approximately -27dB.

These sidelobes are of greater magnitude than the design aim of -30dB. However, the rotation gear used for the measurements has a large metallic structure which is within the pulse length dimension used for the measurements and the measured sidelobes may be due to near-field influences.

## 5. CONCLUSIONS

The array described in this paper uses a large number of transversely driven elements shaded by a Dolph-Chebyshev weighting function. The performance of a single element agrees closely with the theoretical predictions of performance. An iterative elimination and grouping technique was used to reduce the complexity of amplitude shading function, the reduction in sidelobe level being matched to the expected performance resulting from the random amplitude and phase variations of the elements.

## 6. REFERENCES

[1] D. A. BERLINCOURT, D. R. CURRAN & H. JAFFE, 'Piezoelectric and Piezomagnetic Materials and their Function in Transducers' Chapter 3, Physical Acoustics Volume I, Part A, ed. W. P. Mason, Academic Press, 1964.

[2] D. S. BURNETT & W. W. SOROKA, 'Tables of Rectangular Piston Radiation Impedance Functions, with Applications to Sound Transmission Loss through Deep Apertures' J. Acoust. Soc. Am. 51(5 pt.2), 1972, pp1618-1623

[3] D.J. RAMSDALE & R.A. HOWERTON, 'Effect of Element Failure and Random Errors in Amplitude and Phase on the Sidelobe Level of a Linear Array' J. Acoust. Soc. Am. 68(3), Sept 1980, pp901-906

## ACKNOWLEDGEMENT

The authors wish to thank the Admiralty Research Establishment, Portland for their financial encouragement of this work.

# 100 kHz ARRAY USING TRANSVERSELY DRIVEN ELEMENTS AND 2-DIMENSIONAL SHADING

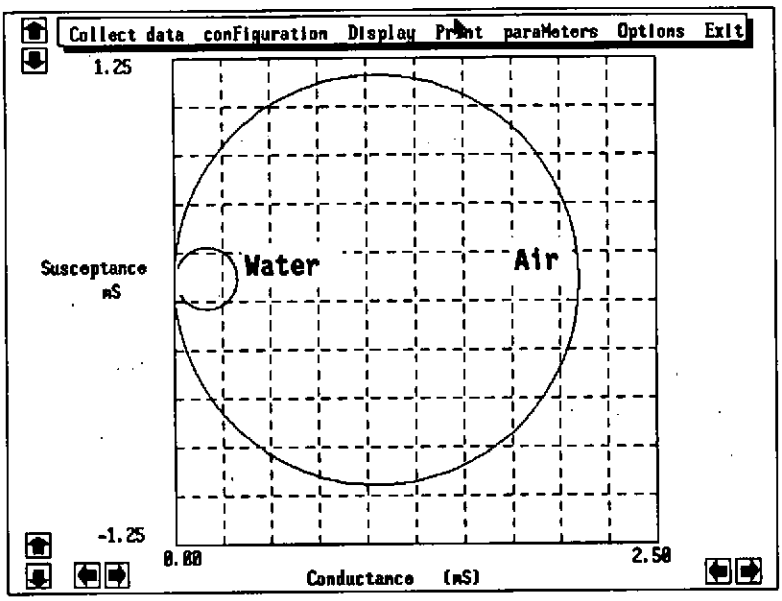


**Figure 1a: Circle Diagram of Unmounted Element**

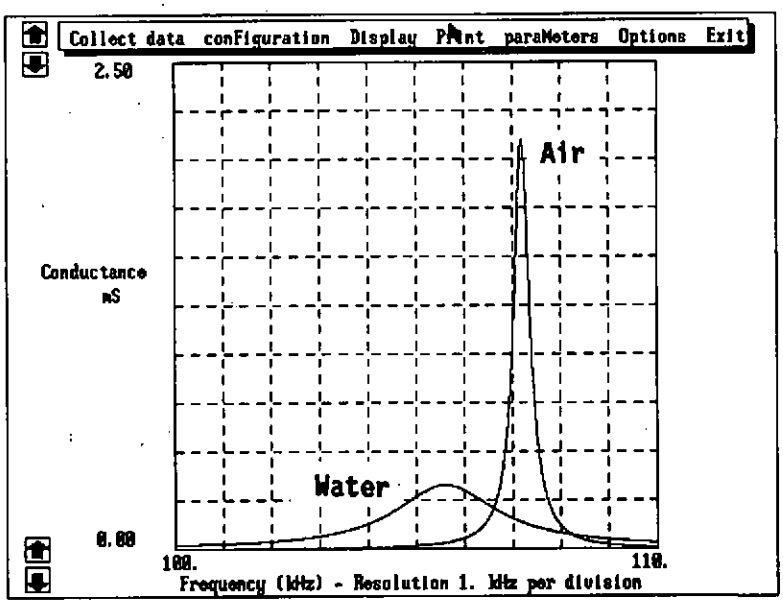


**Figure 1b: Conductance v Frequency of Unmounted Element**

## 100 kHz ARRAY USING TRANSVERSELY DRIVEN ELEMENTS AND 2-DIMENSIONAL SHADING

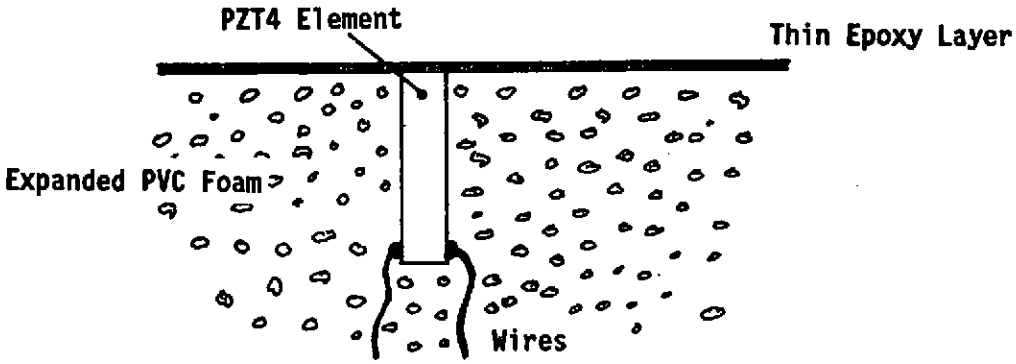


Figure 2: Cross-Section of Element Mounting

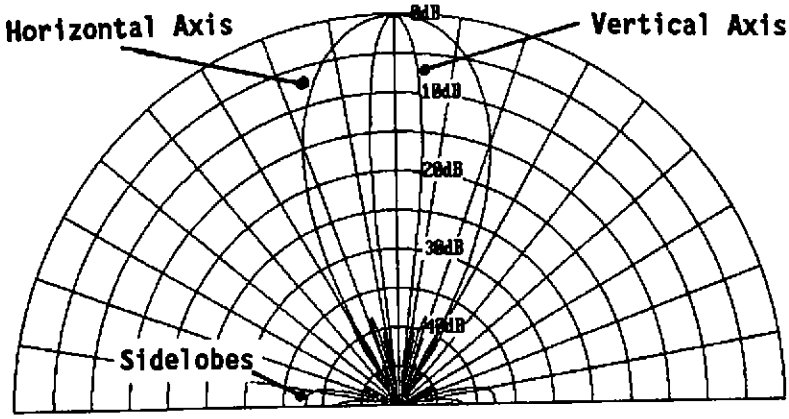


Figure 3: Predicted Beam Pattern After Eliminating and Combining Elements

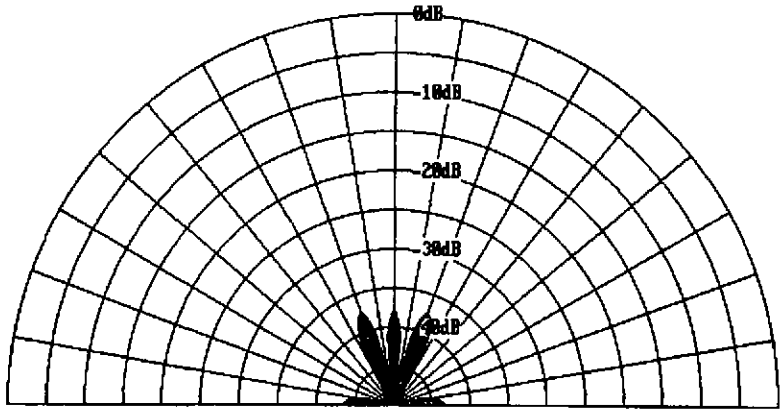


Figure 4: Errors Introduced in the Horizontal Axis

## 100 kHz ARRAY USING TRANSVERSELY DRIVEN ELEMENTS AND 2-DIMENSIONAL SHADING

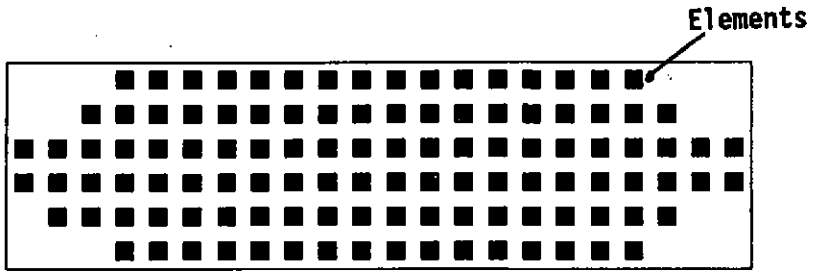


**Figure 5: Final Population of Elements**

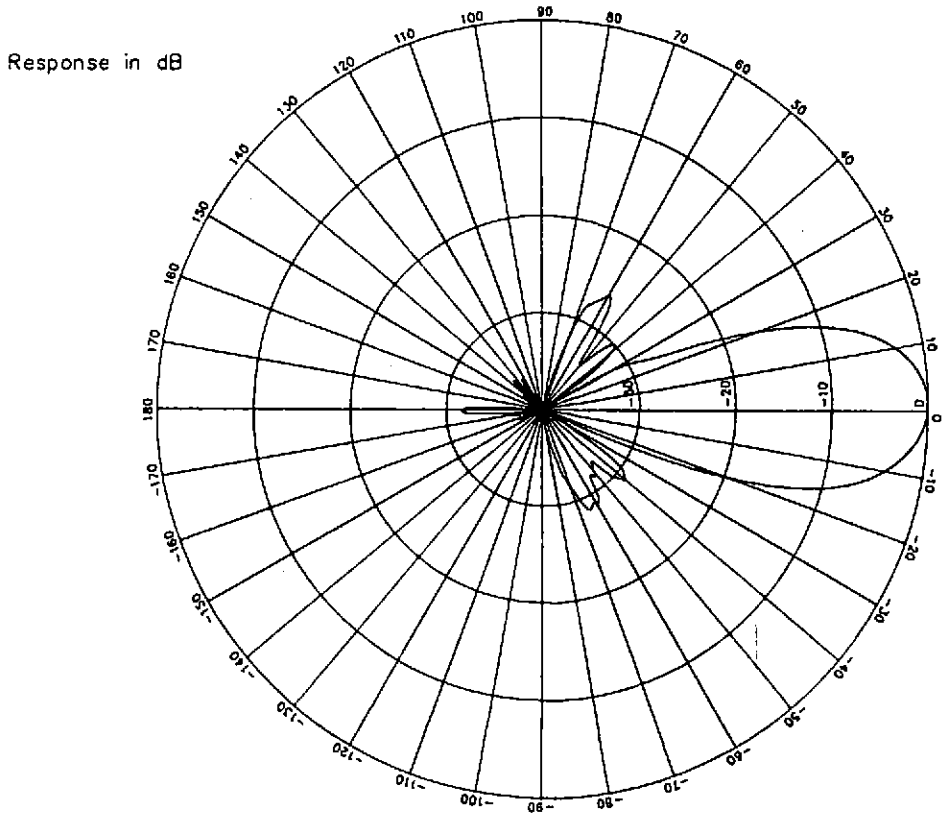


**Figure 6a: Measured Beam Pattern in Horizontal Axis**

## 100 kHz ARRAY USING TRANSVERSELY DRIVEN ELEMENTS AND 2-DIMENSIONAL SHADING

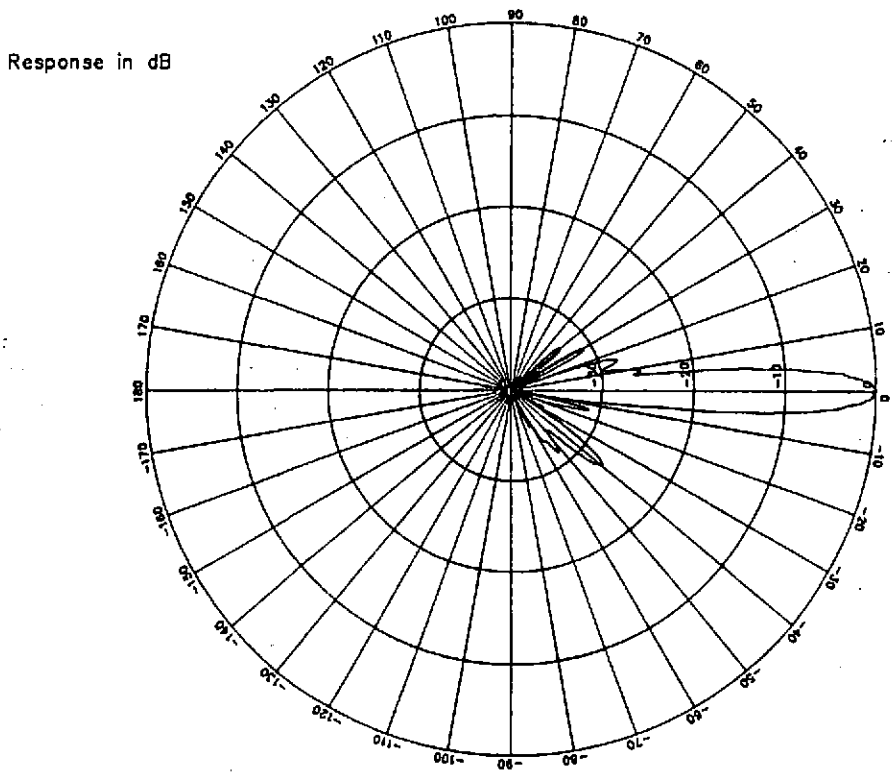


**Figure 6b: Measured Beam Pattern in Vertical Axis**

# NOISE FLOOR OF WIDEBAND PLANAR PVDF TRANSDUCER ARRAYS

Nicholas P. Chotiros and Lewie M. Barber
Applied Research Laboratories
The University of Texas at Austin
Austin, Texas 78713-8029, U.S.A.

## 1. INTRODUCTION

The selfnoise of wideband planar PVDF hydrophones is analysed for the frequency range 1 to 500kHz. The advantages of using PVDF include wideband coverage and simplicity of array construction. Its noise characteristics are different from that of PZT ceramic materials. At certain frequencies PVDF may be more noisy due to limited thickness and a relatively high impedance. Total system selfnoise is dependent on the amplifier chosen. Direct comparisons are made between PVDF and PZT-4 plates. Supporting experimental data are shown.

## 2. INTRINSIC SELFNOISE

The intrinsic noise of the transducer material is represented by the electrical loss tangent. The material parameters used in computing the noise are given in Table I.

TABLE I

| Material | PVDF | PZT-4 |
|---|---|---|
| Manufacturer | Raytheon | Channel Ind. |
| Loss tangent | .015 | .004 |
| Dielectric constant | 29 | 1300 |
| $g_{33}$ (v-m/N) | .50 | .0245 |
| $g_{31}$ (v-m/N) | -.21 | -.0105 |
| $g_{32}$ (v-m/N) | -.03 | -.0105 |
| c - sound speed (m/s) | 1581 | 4166 |

For simplicity, let us consider a simple plate hydrophone one quarter of a wavelength thick. The sensitivity M is given by,

$$M = 0.25 g_h c/f$$

where f is frequency, c the sound speed of the material, and the hydrostatic sensitivity $g_h$ is given by the sum,

$$g_h = g_{33} + g_{31} + g_{32}$$

It is noted that $g_h$ is less than $g_{33}$ because of the negative values in $g_{31}$ and $g_{32}$. In practice, the reduction due to the negative terms may be eliminated. For PZT, this is done with pressure release baffles, and for PVDF by using stiff electrodes. The maximum sensitivity that can be obtained in practice is

$$M = 0.25 g_{33} c/f$$

The equivalent series resistance $R_\theta$ is given by,

$$R_\theta = \left( \frac{\tan(\theta)}{2\pi f C} \right)$$

where tan(θ) is the loss tangent, f the frequency, C the plate capacitance. Hence, the equivalent isotropic noise spectrum level $N_\theta$ is given by

$$N_\theta = 10\mathrm{Log}(4kTR_\theta) - M + DI$$

where k is Boltzmann's constant, T the absolute temperature, and DI the directivity index. The result is independent of plate area because the area terms in C and DI cancel. Intrinsic selfnoise and ocean ambient noise at sea states 0 and 6 are compared in Fig. 1 for $g_h$ and $g_{33}$ sensitivities. By taking the necessary steps to achieve the $g_{33}$ sensitivity, the noise levels of both types of sensors can be made lower than ambient noise.

For the remainder of this paper, the sensitivities given by $g_{33}$ will be assumed since they are clearly the more preferable.

# NOISE FLOOR OF WIDEBAND PLANAR PVDF TRANSDUCER ARRAYS

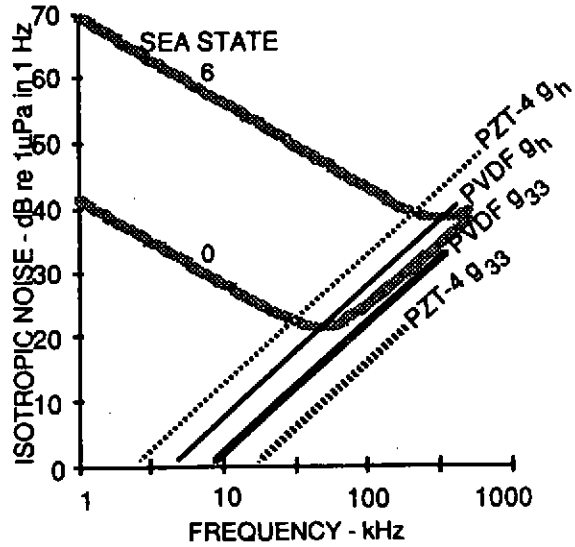


Figure 1. Intrinsic selfnoise of quarter wave plates

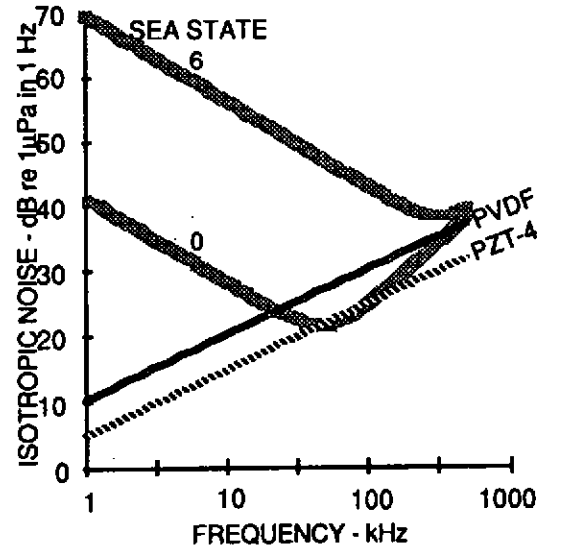


Figure 2. Loss tangent noise of 515μ PVDF and PZT-4 of equivalent thickness

Unlike PZT, the PVDF is only available in a very small selection of thicknesses. The Raytheon PVDF is available as 515μ thick tiles. The loss tangent noise of PVDF is compared to that of PZT of an equivalent thickness in Fig. 2. The thickness limitation raises the intrinsic noise of the PVDF above that of sea state 0 in the band from 20 to 300 kHz.

## 3. WIDEBAND SYSTEM NOISE FLOOR

In narrow and medium bandwidth applications, the intrinsic noise floor is realizable in a hydrophone circuit through the use of resonant networks designed for minimum noise within a specific band. For wideband applications, resonant networks are inappropriate. The transducer must be directly coupled to an amplifier.

Let us consider two representative low noise amplifiers employing bipolar and FET input stages. The selected bipolar device is the LT1028 from Linear Technology. The FET input device is the TLC2201B from Texas Instruments. These devices were selected for their low noise characteristics. The critical specifications of the two amplifiers are shown in Table II.

Table II. Amplifier specifications

| Amplifier | LT1028 | TLC2201B |
|---|---|---|
| Voltage noise - nV/√Hz | 0.9 | 8 |
| Current noise - fA/√Hz | 1000 | 0.6 |
| Input offset current - pA | 25000 | 500 |

The system noise equivalent circuit is shown in Fig. 3. The input offset currents dictate that the input bias resistance $R_b$ not exceed approximately 1MΩ and 50MΩ, for the LT1028 and TLC2201B, respectively; $v_b$ is the thermal noise of the bias resistor; $C_c$ is the capacitance of the conductor between the sensor and amplifier; $v_n$ and $i_n$ are the voltage and current noise sources in the amplifier.

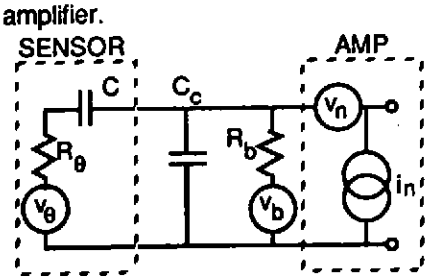


Figure 3. System noise equivalent circuit

NOISE FLOOR OF WIDEBAND PLANAR PVDF TRANSDUCER ARRAYS

### 3.1 HALF-WAVELENGTH APERTURES

Unlike the intrinsic noise, the system noise will not be independent of aperture. Let us start by by examining the system noise at a constant DI, i.e. the aperture varies with the wavelength.

Let us consider a half wavelength square aperture of 515μ PVDF and PZT-4 of an equivalent thickness. Neglecting the conductor capacitance, the equivalent isotropic noise spectrum predicted for the bipolar device is shown in Fig. 4. The system noise is clearly much higher than the intrinsic noise. Above 3 kHz, the noise is particularly high for the PVDF due to a combination of high transducer impedance and high current noise in the bipolar device. The corresponding results for the FET device are shown in Fig. 5. Here the situation is reversed. The PZT-4 circuit is more noisy due to the relatively higher voltage noise of the FET device.

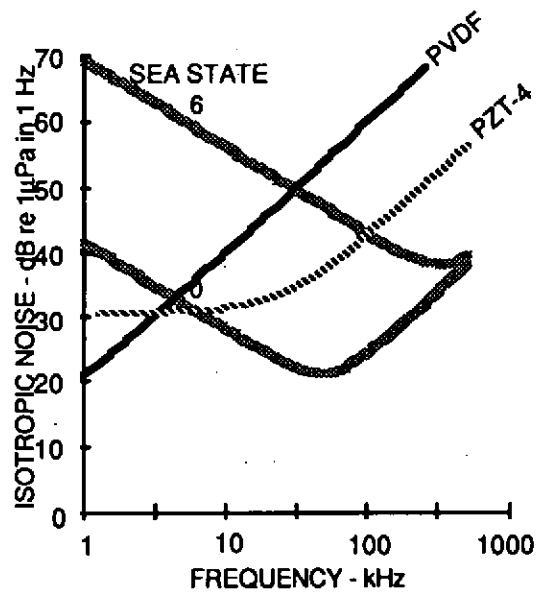


Figure 4. 0.5λ aperture and LT1028 (bipolar ).

In Fig. 6, the two quietest combinations are compared. It appears that, below about 20 kHz, the noise levels are almost identical. At higher frequencies, the PVDF-FET combination is quieter.

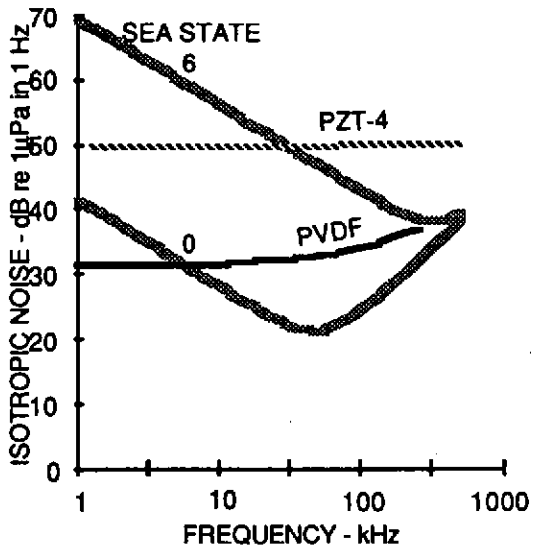


Figure 5. 0.5λ aperture and TLC2201B (FET).

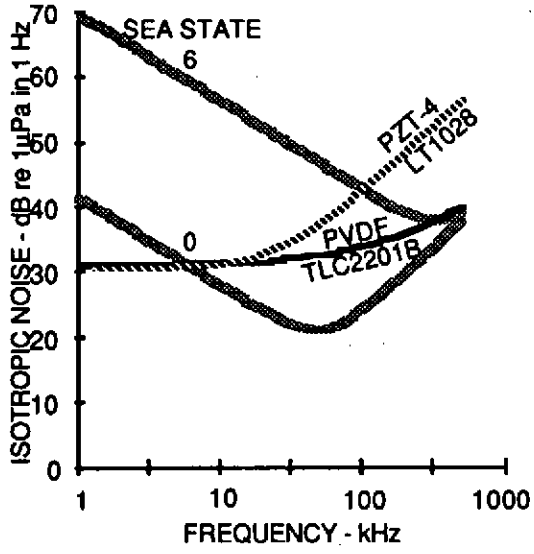


Figure 6. Comparison of 0.5λ aperture PVDF and TLC2201B with PZT-4 and LT1028

Before going on, it is worth noting that above 100kHz, the capacitance of the PVDF half-wavelength square element is quite small. The added capacitance of a 5cm length of shielded twisted pair conductor between sensor and amplifier would have a significant effect on its high

NOISE FLOOR OF WIDEBAND PLANAR PVDF TRANSDUCER ARRAYS

frequency noise floor as shown in Fig. 7. The implication is that for some high frequency applications, it is necessary to integrate sensor and and amplifier. The PZT-4, however, having a much higher dielectric coefficient is unaffected by the added capacitance.

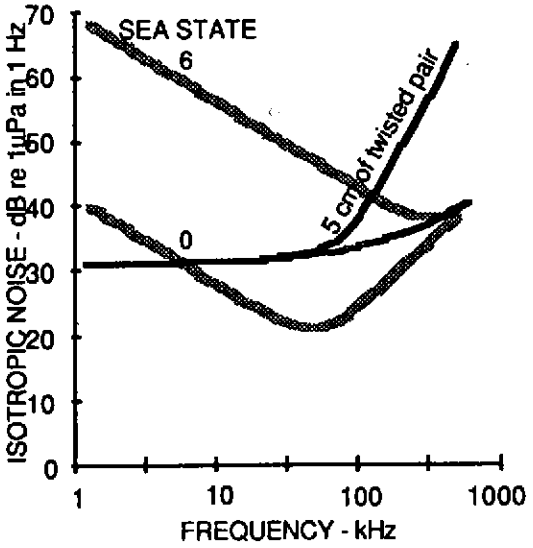


Figure 7. The effect of a 5 cm length of a shielded twisted pair conductor at 250pF/m

## 3.2 LARGER APERTURES

Both the directivity index and capacitance of the sensor are functions of the aperture. It is their interaction with the amplifier noise sources that determines the final system noise floor. As an example, the noise floor of the 4-wavelength square aperture PVDF with bipolar and FET devices are compared in Fig. 8.

In contrast to the half-wavelength aperture, the bipolar device gives lower noise levels over most of the band of interest. Clearly, the intuitive assumption that a FET device should be used with a high impedance sensor such as PVDF is not always correct. The larger apertures give correspondingly larger capacitances, hence lower impedances. The transition between "low" and "high" impedance can occur at quite moderate aperture sizes.

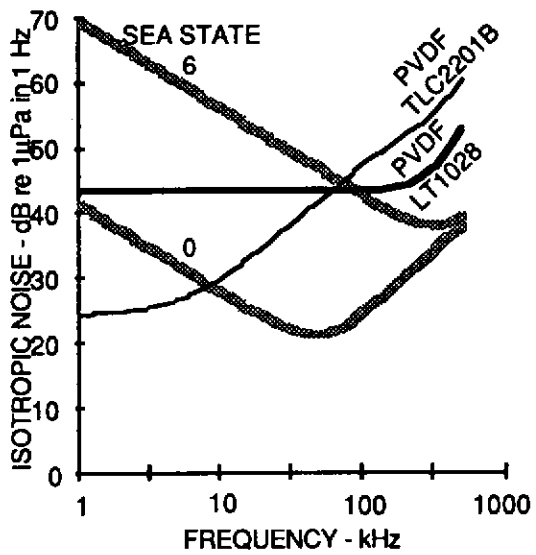


Figure 8. System noise of 4-wavelength square PVDF sensor with TLC2201B and LT1028.

## 3.3 FIXED APERTURES

Finally, let us examine practical cases where the aperture is fixed. For example, consider a 10cm square PVDF plate. Assuming a 5cm length of shielded twisted pair conductor, the predicted system noise with the bipolar and FET devices are compared in Fig. 9. It is seen that above 20 kHz the bipolar device gives the lower noise floor.

A 10 cm square PVDF transducer was constructed and connected to a LT1037 bipolar device, which is similar to but older and noisier than the LT1028. The transducer-amplifier combination was calibrated against a standard hydrophone using a chirp signal. A linear FM chirp covering the band of interest was projected towards the test transducer and the standard. The received signal spectra were computed using standard FFT algorithms. The sensitivity of the test transducer was computed from the difference, in decibels, plus the sensitivity of the standard hydrophone. The system noise was estimated by adding the calculated DI to the measured the output noise spectrum and subtracting the sensitivity. A

NOISE FLOOR OF WIDEBAND PLANAR PVDF TRANSDUCER ARRAYS

comparison of theory and experiment is shown in Fig. 10. The measured noise levels appear to be somewhat higher than the predicted curve. The difference is probably due to other sources of noise in the laboratory.

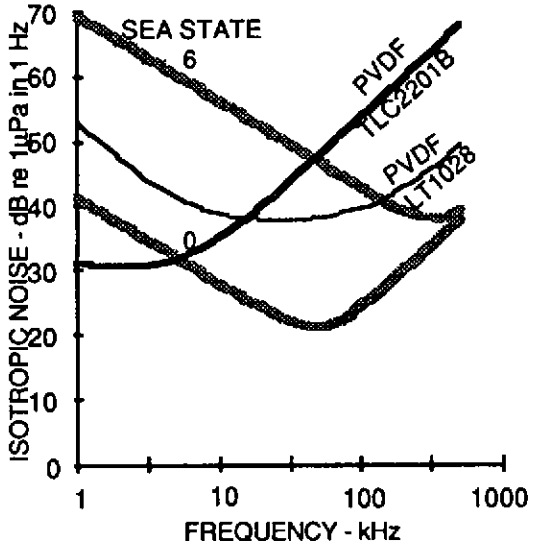


Figure9. System noise of a 1cm square PVDF sensor with TLC2201B and LT1028

## 4. CONCLUSIONS

The intrinsic noise of both PVDF and PZT-4 plates can be reduced below the level of thermal noise. In the case of PVDF, this is accomplished by the use of stiff electrodes; For PZT, it requires pressure release baffling, i.e. air gaps. The PVDF has the disadvantage that it is only available in a few thicknesses, while the need for air gaps may limit the operating depth of the PZT.

The wideband system noise that is obtained when the sensors are directly connected to amplifiers are somewhat higher than the intrinsic noise. Low noise FET and bipolar devices were both examined. The lowest noise combination is a function of the sensitivity and capacitance of the sensors, and the noise characteristics of available amplifiers. The capacitance of the conductor between a PVDF transducer and its amplifier may be a significant factor in certain circumstances.

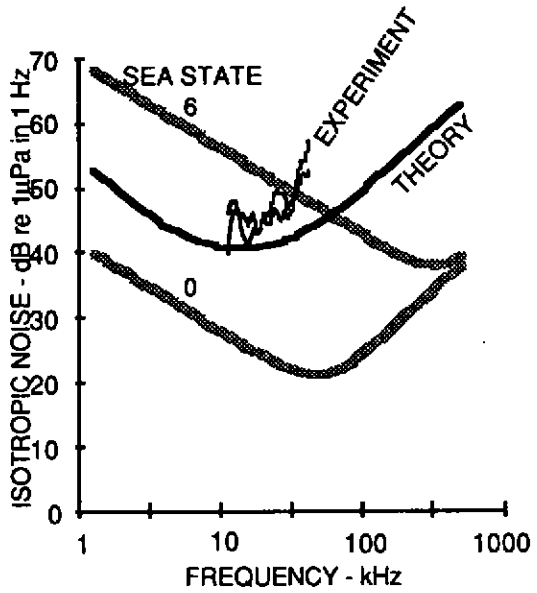


Figure 10. Predicted and measured noise spectra of two samples of 10cm square, 515μ thick PDVF transducers potted in polyurethane and amplified by LT1037 bipolar amplifiers.

## 5. ACKNOWLEDGEMENTS

The work was supported by internal research funds of the Applied Research Laboratories, the University of Texas at Austin. Thanks are due to Tom Muir and Garland Barnard for encouragement. The sensor was assembled by Ken Kirksey. The amplifier was assembled and tested by Carl Faulkner. Data acquisition software was written by Jeff Shorey. Calibration software was written by Rob Stewart. Information regarding sensor behavior and characteristics was supplied by the manufacturers of PVDF and PZT sensor materials, including Raytheon, Pennwalt, EDO and Channel Industries.